

# Radical chemistry in the Pearl River Delta: observations and modeling of OH and HO<sub>2</sub> radicals in Shenzhen 2018

Xinping Yang<sup>1,2</sup>, Keding Lu<sup>1,2,\*</sup>, Xuefei Ma<sup>1,2</sup>, Yue Gao<sup>1,2</sup>, Zhaofeng Tan<sup>3</sup>, Haichao Wang<sup>4</sup>, Xiaorui Chen<sup>1,2</sup>, Xin Li<sup>1,2</sup>, Xiaofeng Huang<sup>5</sup>, Lingyan He<sup>5</sup>, Mengxue Tang<sup>5</sup>, Bo Zhu<sup>5</sup>, Shiyi Chen<sup>1,2</sup>, Huabin Dong<sup>1,2</sup>, Limin Zeng<sup>1,2</sup>, Yuanhang Zhang<sup>1,2,\*</sup>

<sup>1</sup>State Key Joint Laboratory of Environmental Simulation and Pollution Control, College of Environmental Sciences and Engineering, Peking University, Beijing, China

<sup>2</sup>State Environmental Protection Key Laboratory of Atmospheric Ozone Pollution Control, Peking University, Beijing, China

<sup>3</sup>Institute of Energy and Climate Research, IEK-8: Troposphere, Forschungszentrum Juelich GmbH, Juelich, Germany

<sup>4</sup>School of Atmospheric Sciences, Sun Yat-Sen University, Zhuhai, China

<sup>5</sup>Laboratory of Atmospheric Observation Supersite, School of Environment and Energy, Peking University Shenzhen Graduate School, Shenzhen, China

Correspondence to: Keding Lu ([k.lu@pku.edu.cn](mailto:k.lu@pku.edu.cn)), Yuanhang Zhang ([yhzhang@pku.edu.cn](mailto:yhzhang@pku.edu.cn))

**Abstract.** The ambient radical concentrations were measured continuously by laser-induced fluorescence during the STORM (STudy of the Ozone foRmation Mechanism) campaign at the Shenzhen site, located in the Pearl River Delta in China, in autumn 2018. The diurnal maxima were  $4.5 \times 10^6 \text{ cm}^{-3}$  for OH and  $4.5 \times 10^8 \text{ cm}^{-3}$  for HO<sub>2</sub> (including an estimated interference of 23%-28% from RO<sub>2</sub> radicals during the daytime), respectively. The state-of-the-art chemical mechanism underestimated the observed OH concentration, similar to the other warm-season campaigns in China. The OH underestimation was attributable to the missing OH sources, which can be explained by the X mechanism. Good agreement between the observed and modeled OH concentrations was achieved when an additional numerical X equivalent to 0.1 ppb NO concentrations was added to the base model. The isomerization mechanism of RO<sub>2</sub> derived from isoprene contributed approximately 7% to the missing OH sources and the oxidation of isoprene oxidation products (MACR and MVK) had no significant impact on the missing OH sources, demonstrating further exploration of unknown OH sources is necessary. Photolysis reactions dominated the ROx primary production rate. The HONO, O<sub>3</sub>, HCHO, and carbonyls photolysis accounted for 29%, 16%, 16%, and 11% during the daytime, respectively. The ROx termination rate was dominated by the reaction of OH + NO<sub>2</sub> in the morning, and thereafter the radical self-combination gradually became the major sink of ROx in the afternoon. As the sum of the respective oxidation rates of the pollutants via reactions with oxidants, the atmospheric oxidation capacity was evaluated, with a peak of 11.8 ppb h<sup>-1</sup> around noontime. The ratio of  $P(\text{O}_3)$  to  $\text{AOC}_{\text{VOCs}}$ , which indicates the O<sub>3</sub> production from VOCs oxidation, trended to increase and then decrease as the NO concentration increased. Additionally, the maximum of the ratios existed when the NO concentration was approximately 1 ppb, with a median of about 2, indicating that the yield of ozone production from VOCs oxidation was about 2 in this campaign.

## 34 **1 Introduction**

35 Severe ambient ozone ( $O_3$ ) pollution is one of China's most significant environmental challenges, especially in urban areas  
36 (Shu et al., 2020; Li et al., 2019; Wang et al., 2020; Ma et al., 2019b; Wang et al., 2017). Despite the reduction in emissions of  
37  $O_3$  precursors,  $O_3$  concentration is increasing, especially in urban cities. The  $O_3$  average trends for the focus megacity clusters  
38 are 3.1 ppb  $a^{-1}$ , 2.3 ppb  $a^{-1}$ , 0.56 ppb  $a^{-1}$ , and 1.6 ppb  $a^{-1}$  for North China Plain (NCP), Yangtze River Delta (YRD), Pearl River  
39 Delta (PRD), and Szechwan Basin (SCB), respectively (Li et al., 2019). The nonlinearity between  $O_3$  and precursors illustrates  
40 that it is necessary to explore the cause of  $O_3$  production. The tropospheric  $O_3$  is only generated in the photolysis of nitrogen  
41 dioxide ( $NO_2$ ), produced as the by-product within the radical cycling. Thus, the investigation of radical chemistry is critical to  
42 controlling secondary pollution.

43 Hydroxyl radicals (OH), the dominant oxidant, control the atmospheric oxidation capacity (AOC) in the troposphere. The  
44 OH radicals convert primary pollutants to secondary pollutants and are simultaneously transformed into peroxy radicals ( $HO_2$   
45 and  $RO_2$ ). Within the interconvert of  $RO_x$  ( $= OH, HO_2,$  and  $RO_2$ ), secondary pollutants are generated, and thus the further  
46 exploration of radical chemistry is significant. The radical closure experiment, an effective indicator for testing our  
47 understanding of radical chemistry, has been conducted since the central role of OH radicals was recognized in the 1970s (Levy,  
48 1971; Hofzumahaus et al., 2009). The underestimation of OH radicals in environments characterized by low nitrogen oxides  
49 (NO) and high volatile organic compounds (VOCs) has been identified (Lu et al., 2013; Lu et al., 2012; Tan et al., 2017; Tan  
50 et al., 2019; Yang et al., 2021; Hofzumahaus et al., 2009; Lelieveld et al., 2008; Whalley et al., 2011). New radical mechanisms  
51 involving unclassical OH regeneration have been proposed, including Leuven Isoprene Mechanism (LIM) and X mechanism  
52 (Peeters and Muller, 2010; Peeters et al., 2014; Peeters et al., 2009; Hofzumahaus et al., 2009). The LIM has been incorporated  
53 into the current mechanism and is still insufficient to explain the OH missing sources. The X mechanism was identified several  
54 times, but the amount of the numerical species, X, varied in different environments, and the nature of X is unknown  
55 (Hofzumahaus et al., 2009; Lu et al., 2013; Lu et al., 2012; Tan et al., 2017; Tan et al., 2019; Yang et al., 2021). Therefore,  
56 further exploration of radical regeneration sources is necessary.

57 Due to the strong photochemistry influenced by high temperatures, high  $O_3$  pollution appeared to occur in YRD and PRD,  
58 especially in PRD (Ma et al., 2019b; Wang et al., 2017). Radicals, the dominant oxidant in the troposphere, have been measured  
59 during warm seasons in NCP (Yufa 2006, Wangdu 2014, and Beijing 2016), YRD (Taizhou 2018), SCB (Chengdu 2019), and  
60 PRD (Backgarden 2006, and Heshan 2014) in China (Lu et al., 2013; Lu et al., 2012; Tan et al., 2017; Tan et al., 2019; Yang  
61 et al., 2021; Tan et al., 2021). The radical observations in PRD, where the cities are suffering from severe  $O_3$  pollution, have  
62 not been conducted since 2014, and thus the oxidation capacity here has not been clear in recent years. Therefore, we carried  
63 out a continuous comprehensive field campaign (STudy of the Ozone foRmation Mechanism - STORM) involving radical  
64 observations in Shenzhen, one of the megacities in PRD, in autumn 2018. Overall, the following will be reported in this study.

- 65 (1) The observed radical concentrations, and the comparison between the radical observations and simulations.
- 66 (2) The exploration of the unclassical OH regeneration sources based on the experimental budget.
- 67 (3) The sources and sinks of radicals.
- 68 (4) The evaluation of the atmospheric oxidation capacity.

## 69 2 Methodology

### 70 2.1 Measurement site and instrumentation

71 The STORM campaign was conducted from September to October 2018 in Peking University Shenzhen Graduate School  
72 (22.60 deg N, 113.97 deg E), in the west of Shenzhen, Guangdong province. As shown in Fig. 1, this site, which belongs to  
73 the urban site, is located in the university town, and is surrounded by residential and commercial areas. The northwest of the  
74 site is close to the Shenzhen Wildlife Park, and the northeast is close to the Xili Golf Club (Yu et al., 2020). The Tanglang  
75 Mountain Park with active biogenic emissions is located about 1 km southeast of the site. Overall, this site has no significant  
76 local pollution sources nearby, but can represent the urban pollution characteristics (Huang et al., 2012b; Huang et al., 2012a;  
77 Gao et al., 2018).



78  
79 **Figure 1: Geographical location and surrounding environmental conditions of the measurement site in STORM campaign (The**  
80 **maps are from <https://map.baidu.com>).**

81 Most instruments were set up on the top of a four-story academic building (about 20 m). Besides HO<sub>x</sub> radicals measured by  
82 the Peking University Laser-Induced Fluorescence system (PKU-LIF) (see the details in Sect. 2.2), a comprehensive set of  
83 trace gases was conducted to support the exploration of the radical chemistry, including meteorological parameters  
84 (temperature, pressure, relative humidity), photolysis frequency, OH reactivity ( $k_{OH}$ ) and the trace gases (NO, NO<sub>2</sub>, O<sub>3</sub>, VOCs,  
85 *etc.*).  $k_{OH}$  was measured by the laser flash photolysis-laser induced fluorescence (LP-LIF) system. Most of the inorganic trace  
86 gases (O<sub>3</sub>, CO, NO, NO<sub>2</sub>, and SO<sub>2</sub>) were simultaneously measured by two sets of instruments, and good agreement was  
87 achieved within the uncertainty. VOCs (aldehydes, alkenes, aromatics, isoprene, and oxygenated VOCs (OVOCs)) were

88 measured using a gas chromatograph following a mass spectrometer (GC-MS). In addition, HONO and HCHO were measured  
89 as well. Table S1 in the Supplementary Information describes the experimental details of the meteorological and chemical  
90 parameters during this campaign.

## 91 2.2 The OH and HO<sub>2</sub> measurements

92 The OH and HO<sub>2</sub> radicals were measured by Peking University laser-induced fluorescence system (PKU-LIF) based on the  
93 fluorescence assay by gas expansion (FAGE) technique. The principle has been reported in previous studies, only a brief  
94 description of the instrument is presented here. Further detailed information on the instrument can be found in previous studies  
95 (Heard and Pilling, 2003; Fuchs et al., 2008; Holland et al., 1995; Hofzumahaus et al., 1996; Fuchs et al., 2011).

96 In principle, OH resonance fluorescence is released in the OH excitation by a 308 nm pulsed laser, and then OH radicals are  
97 detected directly. HO<sub>2</sub> radicals are converted into OH via NO, and then they are detected. The system contains a laser module  
98 and a detection module. Ambient air was drawn into two independent, parallel, low-pressure (3.5 mBar) cells through two  
99 parallel nozzles with 0.4 mm diameter pinhole. The OH radicals are excited into resonance fluorescence in the OH detection  
100 cell and detected by micro-channel plate detectors (MCP). In the HO<sub>2</sub> detection cell, NO is injected and converts HO<sub>2</sub> to OH  
101 radicals, which then are excited by the laser and release resonance fluorescence. Besides, an OH reference cell in which a large  
102 OH concentration is generated by pyrolysis of water vapor on a hot filament is applied to automatically correct the laser  
103 wavelength.

104 Owing to the failure of the reference cell in this study, the NO mixing ratios injected into the HO<sub>2</sub> cell were set to be higher  
105 than that in other campaigns in China because the HO<sub>2</sub> cell needed to be used as a reference cell to correct laser wavelength.  
106 In this campaign, NO mixing ratios were switched between 25 ppm (low NO mode) and 50 ppm (high NO mode). We  
107 calculated the HO<sub>2</sub> conversion rates under the two different NO concentrations by calibrating the PKU-LIF system. HO<sub>2</sub>  
108 conversion rates in low NO mode ranged within 80%-95%, while those in high NO mode were over 100%, demonstrating that  
109 the HO<sub>2</sub> measurement was affected by RO<sub>2</sub> radicals. Prior studies have reported the relative detection sensitivities ( $\alpha_{RO_2}$ ) for  
110 the major RO<sub>2</sub> species, mainly from alkenes, isoprene and aromatics, when the HO<sub>2</sub> conversion rate was over 100% (Fuchs et  
111 al., 2011; Lu et al., 2012; Lu et al., 2013). Therefore, only the HO<sub>2</sub> observations in high NO mode were chosen and they were  
112 denoted as [HO<sub>2</sub>\*], which was the sum of the true HO<sub>2</sub> concentration and a systematic bias from the mixture of RO<sub>2</sub> species *i*  
113 which were detected with different relative sensitivities  $\alpha_{RO_2}^i$ , as shown in Eq. (1) (Lu et al., 2012). The true HO<sub>2</sub> concentration  
114 was difficult to calculate because the RO<sub>2</sub> concentration measurements and their speciation were not available. Herein, we  
115 simulated the HO<sub>2</sub> and HO<sub>2</sub>\* concentrations by the model. The interference from RO<sub>2</sub> radicals was estimated to be the  
116 difference between the modeled HO<sub>2</sub> and HO<sub>2</sub>\* concentrations.

$$117 \quad [HO_2^*] = [HO_2] + \sum(\alpha_{RO_2}^i \times [RO_2]_i) \quad (1)$$

118 Additionally, prior studies reported that OH measurement might be affected by the potential interference, when the sampled

119 air contained ozone, alkenes and BVOCs (Mao et al., 2012; Fuchs et al., 2016; Novelli et al., 2014), indicating the  
120 environmental conditions are important to the production of interference. The pre-injector is usually used to test the potential  
121 OH interference, and has been applied to our PKU-LIF system to quantify the possible interferences for several campaigns,  
122 including the campaigns conducted in Wangdu, Heshan, Huairou, Taizhou and Chengdu sites (Tan et al., 2017; Tan et al., 2019;  
123 Tan et al., 2018; Yang et al., 2021). No significant internal interference was found in the prior studies, demonstrating the  
124 accuracy of the PKU-LIF system has been determined for several times. Moreover, to further explore the potential interference  
125 in this campaign, we compared the major environmental conditions, especially O<sub>3</sub>, alkenes and isoprene, between Shenzhen  
126 and Wangdu sites, as shown in the Supplementary Information. The environmental condition in Shenzhen was less conducive  
127 to generating interference than that in Wangdu, and the details were presented in the Supplementary Information. Therefore, it  
128 is not expected that the OH measurements in this campaign were affected by the internal interference. Overall, the measurement  
129 uncertainties of OH and HO<sub>2</sub>\* radicals were 11% and 15%, respectively, as shown in Table S1 in the Supplementary  
130 Information.

131

### 132 **2.3 Closure experiment**

133 As an effective tool to explore the atmospheric radical chemistry, the radical closure experiment can investigate the state-of-  
134 the-art chemical mechanism because of the extremely short lifetime of radicals (Stone et al., 2012; Lu et al., 2019). A zero-  
135 dimensional box model was used to conduct the radical closure experiment, and the overall framework was reported by Lu et  
136 al. (2019). In this work, we conducted the radical closure experiment based on the Regional Atmospheric Chemical Mechanism  
137 updated with the latest isoprene chemistry (RACM2-LIM1), as Tan et al. (2017) described in detail. The model was constrained  
138 to the measured meteorological, photolysis frequency, and the critical chemical parameters (CO, NO, NO<sub>2</sub>, VOCs, *etc.*). The  
139 H<sub>2</sub> and CH<sub>4</sub> mixing ratios were set to 550 ppb and 1900 ppb, respectively. The model was operated in time-dependent mode  
140 with a 5-min time resolution, and a 2-d spin-up time was to make the unconstrained species approach the steady state relative  
141 to the constrained species.

142 As Lu et al. (2012) described, there are two types of radical closure experiment. One is the comparison of observed and  
143 modeled radical concentrations, and the other is the comparison of radical production and destruction rates. The most  
144 significant difference between the above is that the latter is conducted with the observed radical concentrations and  $k_{OH}$   
145 constrained. The comparison of radical production and destruction rates, also called radical experimental budget, can test the  
146 accuracy of the state-of-the-art chemistry mechanisms based on the equivalent relationship between the radical production and  
147 destruction rates. The production rates of OH, HO<sub>2</sub>, and RO<sub>2</sub> radicals are quantified from all the known sources. The destruction  
148 rates of HO<sub>2</sub> and RO<sub>2</sub> radicals are the sum of the known sources. The OH destruction rate can be directly calculated as the  
149 product of the observed OH concentrations and the observed  $k_{OH}$  (Tan et al., 2019; Yang et al., 2021). The OH destruction rate

150 is the total sinks of OH radicals because of the direct  $k_{OH}$  observation, and thus the discrepancy between the OH destruction  
151 and production rates denotes the missing OH sources. The detailed reactions and the reaction rate constants related to OH,  
152 HO<sub>2</sub>, and RO<sub>2</sub> radicals can be found in Tan et al. (2019) and Yang et al. (2021).

## 153 2.4 AOC evaluation

154 The life time of the trace gases is controlled not only by the oxidant concentration but also by its second-order rate constant,  
155 so the atmospheric oxidation capacity (AOC) proposed by Geyer et al. (2001) is most suitable to evaluate the relative  
156 importance of each oxidant (Elshorbany et al., 2009). AOC is the core driving force of complex air pollution, and determines  
157 the removal rate of trace gases and the production rates of secondary pollutants (Liu et al., 2021). As an effective indicator for  
158 atmospheric oxidation intensity, the evaluation of AOC can provide crucial information on the atmospheric composition of  
159 harmful and climate forcing species (Elshorbany et al., 2009). AOC is defined as the sum of the respective oxidation rates of  
160 the pollutants via reactions with oxidants (Elshorbany et al., 2009; Geyer et al., 2001; Zhu et al., 2020). According to the  
161 definition of AOC, it can be calculated by the Eq. (2).

$$162 \text{AOC} = \sum_i k_{Y_i}[Y_i][X] \quad (2)$$

163 where  $Y_i$  are the pollutants (CO, CH<sub>4</sub>, and VOCs),  $X$  are the main atmospheric oxidants (OH, O<sub>3</sub>, NO<sub>3</sub>), and  $k_{Y_i}$  is the bi-  
164 molecular rate constant for the reaction of  $Y_i$  with  $X$ . AOC includes all combination of pollutants  $Y$  and oxidants  $X$ . The  
165 higher AOC, the higher removal rate of the most pollutants, and thus the higher production rate of secondary pollutants (Yang  
166 et al., 2020a). Simultaneous measurements of OH and the key trace gases are available in the study. NO<sub>3</sub> concentration could  
167 be simulated by the box model with the observed parameters constrained.

## 168 3. Results

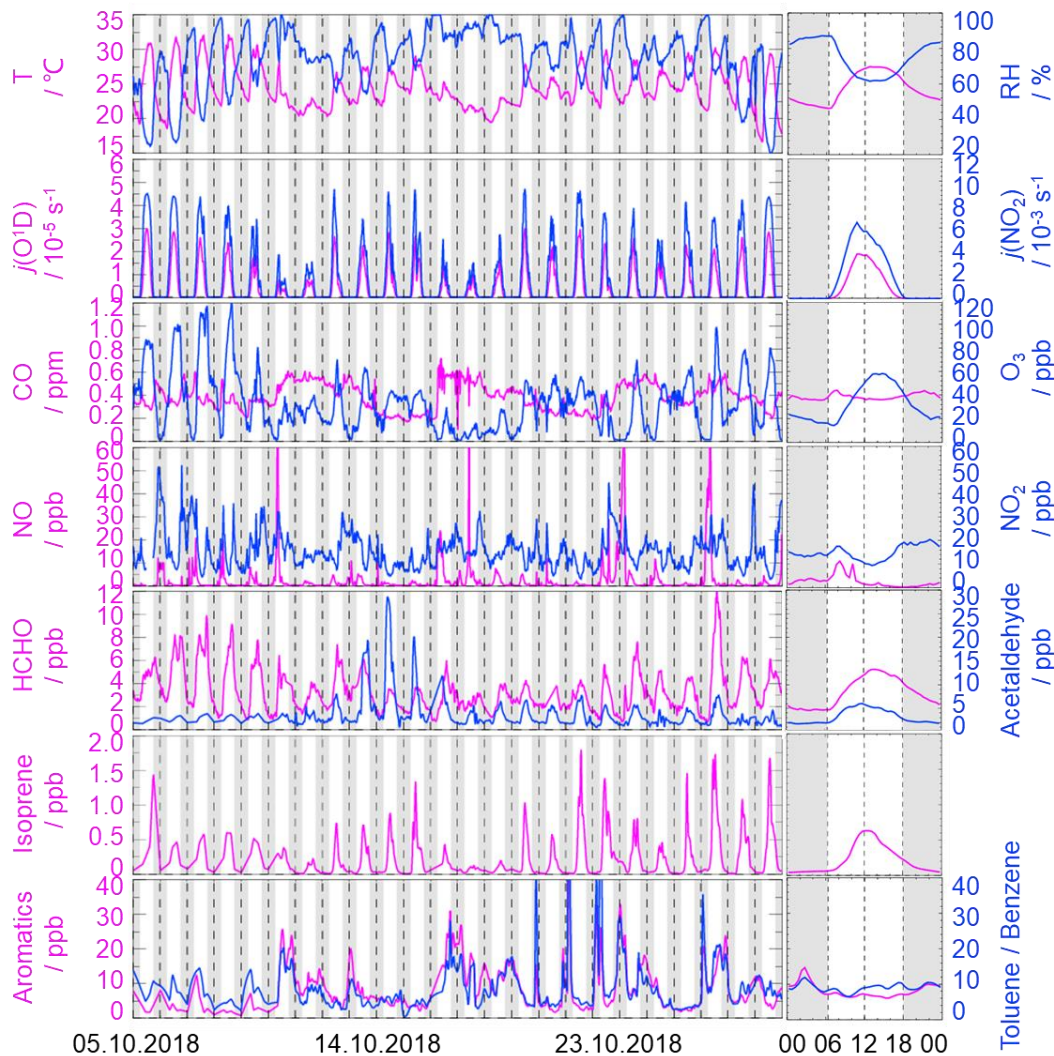
### 169 3.1 Meteorological and chemical conditions

170 Figure 2 gives an overview of the meteorological and chemical parameters from 05 October to 28 October 2018, when OH  
171 and HO<sub>2</sub> radicals were measured. The diurnal variations of the temperature (T), relative humidity (RH),  $j(\text{O}^1\text{D})$ , and  $j(\text{NO}_2)$   
172 followed a regular pattern from day to day. The overall meteorological conditions were characterized by high temperature  
173 (about 20~30 °C), high relative humidity (60~80%), and intensive radiation with  $j(\text{O}^1\text{D})$  up to  $2.0 \times 10^{-5} \text{ s}^{-1}$  and  $j(\text{NO}_2)$  up to  
174  $6.0 \times 10^{-3} \text{ s}^{-1}$ . The relative humidity and photolysis-frequency in this autumn campaign were similar to those in the summer  
175 campaign conducted at Chengdu site (Yang et al., 2021). The temperature in this campaign was lower than that at Chengdu  
176 site, but similar to that in the autumn campaign at Heshan site located in PRD as well (Tan et al., 2019; Yang et al., 2021).

177 The concentration of CO showed weak diurnal variation, indicating there was the non-obvious accumulation of  
178 anthropogenic emissions on a regional scale. NO concentration peaked at 12 ppb during morning rush hour when the traffic

179 emission was severe, and thereafter, O<sub>3</sub> concentration started to increase with the decreasing of NO concentration. The maxima  
180 of O<sub>3</sub> hourly concentration were high up to 120 ppb. According to the updated National Ambient Air Quality Standard of China  
181 (GB3095-2012), O<sub>3</sub> concentration exceeded the Class-II limit values (hourly averaged limit 93 ppb) on several days (6, 7, 8,  
182 and 26 October) when the environmental condition was characterized by high temperature and low relative humidity. NO<sub>2</sub>  
183 concentration was high at night because of the titration effect of O<sub>3</sub> with NO.

184 Along with the high O<sub>3</sub> concentration on 6, 7, 8, and 26 October, high HCHO concentration was also recorded during the  
185 corresponding periods, indicating HCHO was mainly produced as secondary pollutions because of the active photochemistry  
186 in this campaign. Isoprene, mostly derived from biogenic emissions and mainly affected by temperature, peaked around  
187 noontime. Tan et al. (2019) reported the median concentration of HCHO and isoprene concentrations were 6.8 ppb and 0.6 ppb  
188 during 12:00-18:00 at Heshan site. Similarly, the median concentration of HCHO and isoprene concentrations in this study  
189 were 4.9 ppb and 0.4 ppb during the corresponding periods, respectively. As a proxy for traffic intensity, the toluene to benzene  
190 ratio (T/B), which is below 2, means the traffic emissions are the major sources of VOCs (Brocco et al., 1997). The T/B  
191 gradually dropped from 07:00 until it reached the minimum value at 09:00, indicating traffic emission contributed more to  
192 VOCs during morning rush hour than during other periods. However, the T/B, which varied within a range of 7-12, was above  
193 2, and thus VOCs emission during this campaign was mainly from other sectors such as those involving solvent evaporation.



194  
 195 **Figure 2: Timeseries and diurnal profiles of the observed meteorological and chemical parameters in STORM campaign. The grey**  
 196 **areas denote nighttime.**

197 Moreover, we compared the environmental conditions between the Backgarden (rural site), Heshan (suburban site), and  
 198 Shenzhen (urban site) campaigns conducted in PRD in Table S3 in the Supplementary Information. No significant discrepancy  
 199 in temperature was found in the Shenzhen and Heshan campaigns, which were both conducted in autumn. The temperature in  
 200 the Backgarden campaign conducted in summer was higher than those in Shenzhen and Heshan. The relative humidity in  
 201 Shenzhen and Backgarden was higher than that in Heshan. Compared to the chemical conditions in the Heshan campaign  
 202 conducted in autumn as well, the concentrations of CO, NO, NO<sub>2</sub>, HONO, alkenes, aromatics, and HCHO in Shenzhen were  
 203 lower, which might be because there were no significant local pollution sources nearby in the Shenzhen site although it was  
 204 an urban site. However, the concentration of O<sub>3</sub> which is the typical secondary pollutant in Shenzhen was higher than that in  
 205 Heshan. Compared to the environmental conditions in Heshan, the higher O<sub>3</sub> concentration in Shenzhen might benefit from  
 206 the weather condition which was characterized by the stronger solar radiation and slightly higher temperatures.

### 207 3.2 Observed and modeled OH and HO<sub>2</sub> radicals

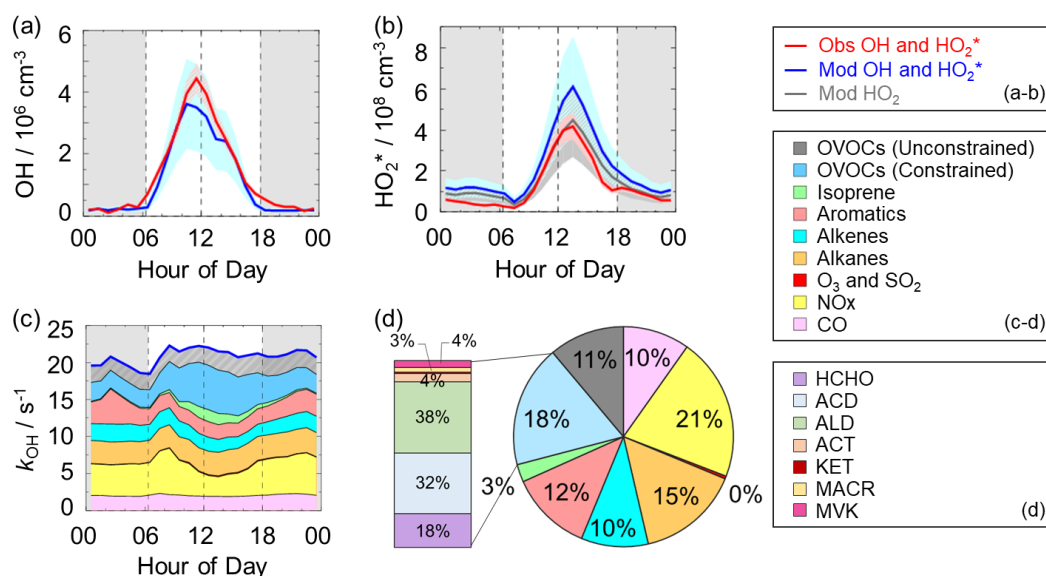
208 The OH and HO<sub>2</sub> radicals were measured during 05-28 October 2018. The timeseries of the observed and modeled HOx  
 209 concentrations are displayed in Fig. S1 (a-b) in the Supplementary Information. Data gaps were caused by the rain, calibration,



210 and maintenance. The daily maxima of the observed OH and HO<sub>2</sub><sup>\*</sup> concentrations varied in the range of (2-9) × 10<sup>6</sup> cm<sup>-3</sup> and  
 211 (2-14) × 10<sup>8</sup> cm<sup>-3</sup>, respectively. As in previous campaigns, the largest OH concentrations appeared around noontime and  
 212 showed a high correlation with j(O<sup>1</sup>D), a proxy for the solar UV radiation driving much of the primary radical production (Tan  
 213 et al., 2019).

214 Figure 3 (a-b) shows the diurnal profiles of the observed and modeled HO<sub>x</sub> concentrations. The HO<sub>x</sub> radicals showed similar  
 215 diurnal behavior to those reported in other campaigns (Ma et al., 2019a; Tan et al., 2017; Tan et al., 2019; Tan et al., 2018;  
 216 Yang et al., 2021). The observed OH and HO<sub>2</sub><sup>\*</sup> concentrations reached a maximum around 12:00 and 13:30, respectively. The  
 217 diurnal maxima of the observed and modeled OH concentrations were 4.5 × 10<sup>6</sup> cm<sup>-3</sup> and 3.5 × 10<sup>6</sup> cm<sup>-3</sup>. Compared to the  
 218 other campaigns conducted in PRD (Backgarden and Heshan), the diurnal maximum of the observed OH concentration in  
 219 Shenzhen was equal to that observed in Heshan, and much lower than that observed in Backgarden where the observed OH  
 220 concentration was nearly 15 × 10<sup>6</sup> cm<sup>-3</sup> (Hofzumahaus et al., 2009; Tan et al., 2019). The higher OH concentration in  
 221 Backgarden site was closely correlated to the stronger solar radiation, as shown in Table S3 in the Supplementary Information.  
 222 The diurnal observed and modeled OH concentrations agreed within their 1-σ uncertainties of measurement and simulation  
 223 (11% and 40%). However, when the NO mixing ratio (Fig. 2) dropped from 10:00 gradually, a systematic difference existed,  
 224 with the observed OH concentration being about 1 × 10<sup>6</sup> cm<sup>-3</sup> higher than the modeled OH concentration. The OH  
 225 concentrations observed in the environments with low NO levels were underestimated by the state-of-the-art models at  
 226 Backgarden (summer) and Heshan (autumn) sites in PRD as well, and the OH underestimation was identified to be universal  
 227 at low NO conditions in China (Lu et al., 2013; Lu et al., 2012; Ma et al., 2019a; Tan et al., 2017; Yang et al., 2021). The  
 228 reasons on OH underestimation was further discussed in Section 4.1.

229



230  
 231 **Figure 3: (a-b) The diurnal profiles of the observed and modeled OH, HO<sub>2</sub><sup>\*</sup> and HO<sub>2</sub> concentrations. (c) The diurnal profiles of the**  
 232 **modeled k<sub>OH</sub>. (d) The composition of the modeled k<sub>OH</sub>. The red areas in (a-b) denote 1-σ uncertainties of the observed OH and HO<sub>2</sub><sup>\*</sup>**

233 concentrations. The blue areas in (a-b) denote 1- $\sigma$  uncertainties of the modeled OH and HO<sub>2</sub><sup>\*</sup> concentrations, and the grey area in  
234 (b) denotes 1- $\sigma$  uncertainties of the modeled HO<sub>2</sub> concentrations. The grey areas in (a-c) denote nighttime. ACD denotes  
235 acetaldehydes. ALD denotes the C3 and higher aldehydes. ACT and KET denote acetone and ketones. MACR and MVK denote  
236 methacrolein and methyl vinyl ketone.

237 The diurnal maximum of the observed HO<sub>2</sub><sup>\*</sup>, the modeled HO<sub>2</sub><sup>\*</sup> and the modeled HO<sub>2</sub> concentrations were  $4.2 \times 10^8 \text{ cm}^{-3}$ ,  
238  $6.1 \times 10^8 \text{ cm}^{-3}$ , and  $4.4 \times 10^8 \text{ cm}^{-3}$ , respectively. The difference between the modeled HO<sub>2</sub><sup>\*</sup> and HO<sub>2</sub> concentrations can be  
239 considered a modeled HO<sub>2</sub> interference from RO<sub>2</sub> (Lu et al., 2012). The RO<sub>2</sub> interference was small in the morning, while it  
240 became larger in the afternoon. It ranged within 23%-28% during the daytime (08:00-17:00), which was comparable with  
241 those in the Backgarden and Yufa sites in China, Borneo rainforest in Malaysia (OP3 campaign, aircraft), and UK (RONOCO  
242 campaign, aircraft) (Lu et al., 2012; Lu et al., 2013; Jones et al., 2011; Stone et al., 2014). The observed HO<sub>2</sub><sup>\*</sup> was  
243 overestimated by the model, indicating the HO<sub>2</sub> heterogeneous uptake might have a significant impact during this campaign.  
244 The diurnal maximum of HO<sub>2</sub><sup>\*</sup> concentration observed in Shenzhen was much lower than those observed in the Yufa and  
245 Backgarden sites (Hofzumahaus et al., 2009; Lu et al., 2012; Lu et al., 2013). The high modeled HO<sub>2</sub>/OH ratio around noontime  
246 (11:00-15:00), which was about 138, was found in this campaign, which was higher than those in the Backgarden and Chengdu  
247 sites (Yang et al., 2021; Hofzumahaus et al., 2009). High HO<sub>2</sub>/OH ratio is normally found only in clean air at low concentrations  
248 of NO<sub>x</sub> (Hofzumahaus et al., 2009; Stevens et al., 1997). As an indicator that can reflect the interconversion reaction between  
249 HO<sub>2</sub> and OH, the conversion efficiency in this campaign was slightly slower than that in the Backgarden and Chengdu sites.

### 250 3.3 OH reactivity

251  $k_{\text{OH}}$  is the pseudo-first-order loss rate coefficient of OH radicals, and it is equivalent to the reciprocal OH lifetime (Fuchs et  
252 al., 2017; Lou et al., 2010; Yang et al., 2019). In this campaign,  $k_{\text{OH}}$  was measured only for several days (05-19 October 2018)  
253 by the LIP-LIF system, which has been reported in the previous study (Liu et al., 2019). The timeseries of the observed and  
254 modeled  $k_{\text{OH}}$  during 05-19 October 2018 are presented in Fig. S2 in the Supplementary Information. A good agreement between  
255 the observed  $k_{\text{OH}}$  and modeled  $k_{\text{OH}}$  within the uncertainties was achieved, and thus the model can be believed to reproduce the  
256 observed  $k_{\text{OH}}$  values within the whole campaign. Moreover, to reflect the  $k_{\text{OH}}$  in the whole campaign, the modeled values were  
257 shown in the  $k_{\text{OH}}$  diurnal profiles (Fig. 3c) during 05-28 October 2018. The modeled  $k_{\text{OH}}$  showed weak diurnal variation and  
258 varied from  $18 \text{ s}^{-1}$  to  $22 \text{ s}^{-1}$ . Compared to the  $k_{\text{OH}}$  variation in Shenzhen, the  $k_{\text{OH}}$  observed in Backgarden and Heshan sites in  
259 PRD showed a stronger diurnal variation, with a minimum value at around noontime and a maximum value at daybreak. The  
260  $k_{\text{OH}}$  ranges in Backgarden and Heshan sites were  $20\text{-}50 \text{ s}^{-1}$  and  $22\text{-}32 \text{ s}^{-1}$  (Lou et al., 2010; Tan et al., 2019). Similar with the  
261 good agreement between the observed and modeled  $k_{\text{OH}}$  during the several days in Shenzhen, the observed  $k_{\text{OH}}$  in Backgarden  
262 was matched well with the modeled  $k_{\text{OH}}$  which has included the OVOCs reactivity. In terms of the  $k_{\text{OH}}$  in Heshan, Tan et al.  
263 (2019) reported that only half of the observed  $k_{\text{OH}}$  was explained by the calculated  $k_{\text{OH}}$  which was calculated from the measured

264 trace gas concentrations. The missing  $k_{OH}$  in Heshan was likely caused by unmeasured VOCs, demonstrating the necessary to  
265 measure more abundant VOCs species, especially OVOCs species.

266 As shown in Fig. 3(d), we presented the composition of modeled  $k_{OH}$ . The inorganic compounds contributed approximately  
267 31% to  $k_{OH}$ , in which the CO and NO<sub>x</sub> reactivity accounted for 10% and 21%, respectively. The NO<sub>x</sub> reactivity was displayed  
268 versus time, with a maximum during the morning peak. The peak concentration during the morning peak was associated with  
269 traffic emissions.

270 Compared with the inorganics reactivity, the larger fraction of  $k_{OH}$  came from the VOCs group, with a contribution of 69%  
271 to  $k_{OH}$ . The contribution of alkanes, alkenes, and aromatics were 15%, 10%, and 12%, respectively. The isoprene reactivity  
272 related to temperature was mainly concentrated during the daytime, whereas the aromatics reactivity at night was higher. As  
273 for the OVOCs species, we measured several OVOCs species, including HCHO, acetaldehydes (ACD) and higher aldehydes  
274 (ALD), acetone (ACT), ketones (KET) and isoprene oxidation products (MACR and MVK), so we constrained these species  
275 in the model. The constrained OVOCs species accounted for 18% in the total  $k_{OH}$ , where HCHO, ACD, and ALD were the  
276 major contributors, with contributions of 18%, 32%, and 38% to the constrained OVOCs, respectively. The contribution of  
277 aldehydes in this study (16%) was larger than that in Beijing (Whalley et al., 2021) and smaller with that in Wangdu (Fuchs et  
278 al., 2017). The remaining reactivity was attributed to the unconstrained OVOCs reactivity, which came from the model-  
279 generated intermediate species (glyoxal, methylglyoxal, methyl ethyl ketone, methanol, etc.), with a contribution of 11% to  
280 the total  $k_{OH}$ . Large fraction of OVOCs reactivities in  $k_{OH}$  was also found in some previous studies (Lou et al., 2010; Lu et al.,  
281 2013; Fuchs et al., 2017; Whalley et al., 2021). About 50% of  $k_{OH}$  was explained by OVOCs in Backgarden site, and HCHO,  
282 ACD and ALD, and oxygenated isoprene products were the most important OH reactants in OVOCs, with a contribution of  
283 30-40%, and other 10-20% came from other oxygenated compounds (ketones, dicarbonyl compounds, alcohols,  
284 hydroperoxides, nitrates etc.) (Lou et al., 2010). HCHO, ACD, MVK, MVCR and glyoxal accounted for one-third of the total  
285  $k_{OH}$  in Wangdu site (Fuchs et al., 2017). The large unconstrained OVOCs reactivity indicated it is necessary to measure more  
286 VOCs species in the future.

## 287 **4. Discussion**

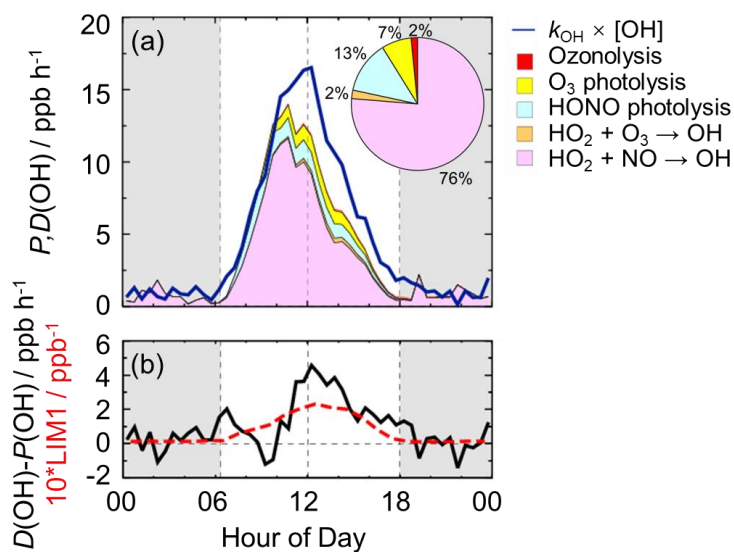
### 288 **4.1 Radical closure experiment**

289 In this study, we conducted OH radical closure experiment which is called OH experimental budget as well. As discussed in  
290 Section 3.3, it is believed that the model can reproduce the observed  $k_{OH}$ . Herein, to conduct the OH experiment budget in the  
291 whole campaign, we used the modeled  $k_{OH}$  to calculate the OH destruction rate because the  $k_{OH}$  was only measured on several  
292 days. The diurnal profiles of OH production and destruction rates, and compositions of OH production rate were displayed in  
293 Fig. 4, with maxima of 14 ppb h<sup>-1</sup> and 17 ppb h<sup>-1</sup> around noontime, respectively. The OH production rate from known sources

294 is quantified from the primary sources (photolysis of HONO, photolysis of O<sub>3</sub>, ozonolysis of alkenes) and secondary sources  
 295 (dominated by HO<sub>2</sub> + NO, and HO<sub>2</sub> + O<sub>3</sub>). The primary and secondary sources were account for 78% and 22% of the total  
 296 calculated production rate, respectively. Similar with the prior studies, the largest fraction of OH production rate comes from  
 297 HO<sub>2</sub> + NO, with a contribution up to 76% of the known OH production rate. The contributions of HONO and O<sub>3</sub> photolysis  
 298 were 13% and 7% to the primary production rate.

299 The OH production rate matched well with the destruction rate only in the early morning to about 10:00. Thereafter, the OH  
 300 destruction rate was larger than the production rate, which could explain the underestimation of OH concentration by the model.  
 301 The discrepancy between the OH production and destruction rates was attributed the missing OH sources. The biggest  
 302 additional OH source was approximately 4.6 ppb h<sup>-1</sup>, which occurred at about 12:00, when the OH production and destruction  
 303 rates were 11.9 ppb h<sup>-1</sup> and 16.5 ppb h<sup>-1</sup>, respectively. The unknown OH source accounted for about one third of the total OH  
 304 production rate, indicating the exploration of missing OH source was significant to study the radical chemistry. It is noted that  
 305 the OH production rate was overestimated because we used HO<sub>2</sub><sup>\*</sup> concentrations instead of HO<sub>2</sub> concentrations here. Thus,  
 306 the missing OH source was the lower limit here, demonstrating more unknown OH sources need to be further explored. Details  
 307 on unknown OH sources are given below (Sect. 4.2).

308



309

310 **Figure 4: (a) The diurnal profiles of OH production and destruction rates and the proportions of different known sources in the**  
 311 **calculated production rate during the daytime. The blue line denotes the OH destruction rate, and the colored areas denote the**  
 312 **calculated OH production rates from the known sources. (b) The missing OH source which was the discrepancy between the OH**  
 313 **destruction and production rates, and the OH production rate which was ten times the production rate derived from LIM1**  
 314 **mechanism. The grey areas denote nighttime.**

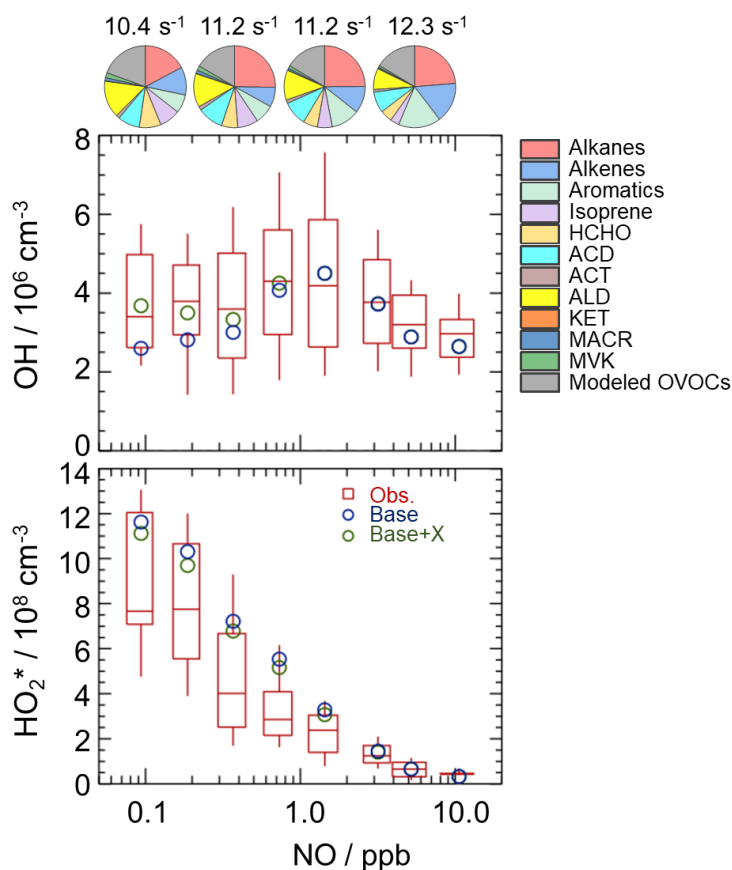
## 315 4.2 Radical chemistry in low NO regime

### 316 4.2.1 Influencing factors of OH underestimation

317 As analyzed in Sect. 4.1, the underestimation of OH concentration was attributable to the missing OH source. It is necessary

318 to explore the influencing factor for gaining further insight into the missing source. Scientists reported that more significant  
 319 OH underestimation would appear with the decreasing NO concentration and increasing isoprene concentration (Lu et al.,  
 320 2012; Ren et al., 2008; Hofzumahaus et al., 2009; Lelieveld et al., 2008; Whalley et al., 2011; Tan et al., 2017; Yang et al.,  
 321 2021). Herein, we further explored the effect of NO concentration on missing OH source. NO dependence of OH and HO<sub>2</sub>  
 322 radicals was illustrated in Fig. 5. The OH concentrations were normalized by the averaged  $j(O^1D)$  to eliminate the influence  
 323 of radiation on radicals. The OH concentration showed an increasing trend with the increase of NO concentrations in low NO  
 324 regime (below 1 ppb) due to the increased OH radicals from propagation via peroxy reactions with NO, and then decreased  
 325 with the increase of NO concentrations in high NO regime (above 1 ppb) due to the loss by the reaction of OH with NO<sub>2</sub>  
 326 (Ehhalt, 1999). The base model can reproduce the observed OH concentration in high NO regime and underestimate OH  
 327 concentration in low NO regime. As for HO<sub>2</sub><sup>\*</sup> radicals, the observed and modeled HO<sub>2</sub><sup>\*</sup> concentrations decreased with the  
 328 increase of NO concentrations. The model overestimated the observations, indicating the heterogeneous uptake might make a  
 329 significant role in HO<sub>2</sub> sinks in this campaign. Overall, NO<sub>x</sub> (= NO + NO<sub>2</sub>) plays a crucial role in radical chemistry due to the  
 330 impact of NO on radical propagation and termination reactions.

331



332

333 **Figure 5: NO dependence of OH and HO<sub>2</sub><sup>\*</sup> radicals. The red box-whisker plots give the 10%, 25%, median, 75%, and 90% of the**  
 334 **HO<sub>x</sub> observations. The blue circles show the median values of the HO<sub>x</sub> simulations by the base model, and the green circles show**  
 335 **the HO<sub>x</sub> simulations by the model with X mechanism. Total VOCs reactivity and their organic speciation are presented by pie charts**  
 336 **at the different NO intervals at the top. Only daytime values and NO concentration above the detection limit of the instrument were**

337 chosen. ACD and ACT denote acetaldehyde and acetone, respectively. ALD denotes the C3 and higher aldehydes. KET denotes  
338 ketones. MACR and MVK, which are both the isoprene oxidation products, denote methacrolein and methyl vinyl ketone,  
339 respectively.

340 To further explore the influencing factors of OH underestimation, we presented the speciation VOCs reactivity under the  
341 different NO intervals, as shown in Fig. 5 and Table S4 in the Supplementary Information. The isoprene reactivity and total  
342 OVOCs reactivity (the sum of HCHO, ACD, ACT, ALD, KET, MACR, MVK and the modeled OVOCs) increased with the  
343 decrease of NO concentrations, while the anthropogenic VOCs reactivity (alkanes, alkenes and aromatics) was higher in high  
344 NO regime. Additionally, the O<sub>3</sub> concentration in low NO regime was significantly higher than those in high NO regime, and  
345 the temperature was slightly higher in low NO regime, demonstrating the photochemistry was more active in low NO regime  
346 in this campaign. Overall, the photochemistry and composition of VOCs reactivity, especially the isoprene and OVOCs species  
347 (mainly ACD, ACT and the modeled OVOCs), might closely impact the missing OH sources.

#### 348 4.2.2 Quantification of missing OH sources

349 Hofzumahaus et al. (2009) proposed an existence of a pathway for the regeneration of OH independent of NO, including the  
350 conversions of RO<sub>2</sub> → HO<sub>2</sub> and HO<sub>2</sub> → OH by a numerical species called X. With a retrospective analysis, the unclassical  
351 OH recycling pathway was identified to be universal at low NO conditions in China. The amount of X varies with  
352 environmental conditions, and the X concentrations were 0.85 ppb, 0.4 ppb, 0.1 ppb, 0.4 ppb, and 0.25 ppb at Backgarden,  
353 Yufa, Wangdu, Heshan, and Chengdu sites (Hofzumahaus et al., 2009; Lu et al., 2012; Lu et al., 2013; Tan et al., 2017; Yang  
354 et al., 2021).

355 In this study, we tested this unclassical X mechanism. Good agreement between observations and simulations of OH radicals  
356 was achieved when a constant mixing ratio of 0.1 ppb of X was added into the base model. As shown in Fig. 5, the model with  
357 X mechanism agreed with the observed OH concentrations even at low NO conditions. Unclassical OH recycling was identified  
358 again in this study. However, X is an artificial species that behaves like NO, and thus the nature of X is still unknown to us.  
359 Compared to Shenzhen site, the required X concentration in the Backgarden and Heshan sites in PRD were higher, which  
360 might be affected by the different air masses in the three sites. The  $k_{OH}$  in Shenzhen site was much lower than those in  
361 Backgarden and Heshan sites, and the weaker diurnal variation of  $k_{OH}$  in Shenzhen was observed. Under the influence of the  
362 East Asian monsoon, the prevailing wind for PRD area is mostly southerly during the summer months and mostly northerly  
363 during the winter months (Fan et al., 2005; Zhang et al., 2008). The Backgarden site is located in Guangzhou, and the Heshan  
364 site is located in Jiangmen. The two cities are along the north-south axis, and thus the air masses of the Backgarden and Heshan  
365 sites are intimately linked with each other, while the air mass in Shenzhen is more similar to Hongkong (Zhang et al., 2008).  
366 Therefore, further exploration on this unclassical OH recycling is needed to improve our understanding of radical chemistry.

367 As discussed in Section 4.2.1, isoprene and OVOCs might have potential influence on the missing OH source. RO<sub>2</sub>

368 isomerization reactions have also been shown to be of importance for the atmospheric fate of RO<sub>2</sub> from isoprene (Peeters et  
369 al., 2009; Peeters et al., 2014). The latest isoprene isomerization mechanism, which is called LIM1, has been coupled into our  
370 current base model. However, LIM1 mechanism was not included in the OH experimental budget which was conducted with  
371 the observations constrained, as shown in Section 4.1. Herein, we evaluated the contribution of LIM1 mechanism to the missing  
372 OH sources, as shown in Fig. 4 (b). LIM1 mechanism can explain approximately 7% of the missing OH sources during 10:00-  
373 16:00, when the missing OH production rate and the OH production rate derived from LIM1 mechanism were 2.47 ppb h<sup>-1</sup> and  
374 0.17 ppb h<sup>-1</sup>, respectively.

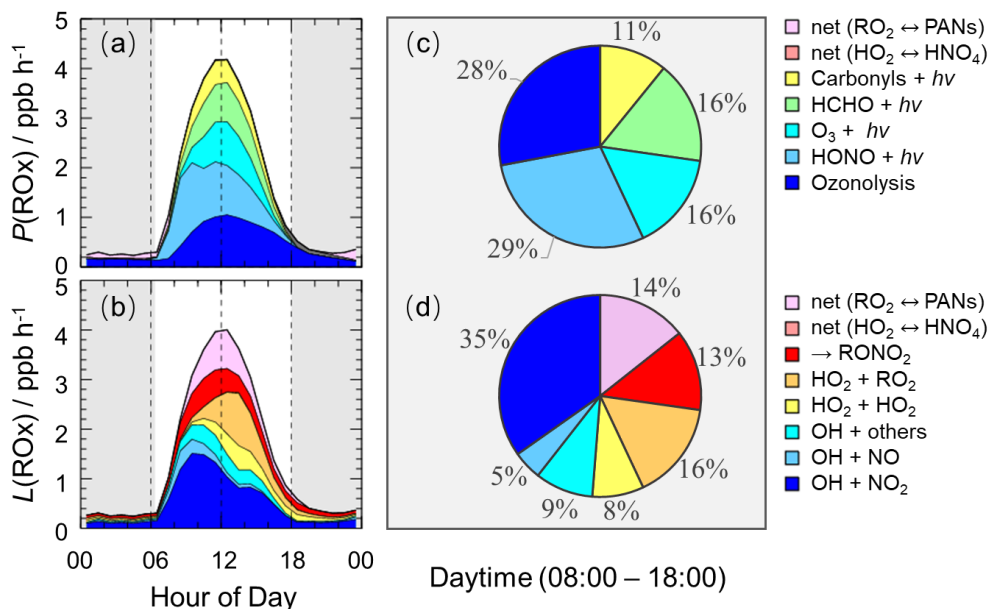
375 Additionally, prior studies also reported that OH regeneration might be achieved from the oxidation of MACR and MVK,  
376 which are the major first-generated products of isoprene (Fuchs et al., 2018; Fuchs et al., 2014). As a potential explanation for  
377 the high OH concentration, the impacts of MACR and MVK oxidation were evaluated here. The modification of MACR  
378 oxidation scheme added the H-migration reactions of MACR oxidation products (Fuchs et al., 2014). The modification of  
379 MVK oxidation scheme added the reactions of MVK oxidation products with HO<sub>2</sub> radicals and the H-migration reactions of  
380 MVK oxidation products (Fuchs et al., 2018). As presented in Fig. S3 in the Supplementary Information, no significant of the  
381 MACR and MVK oxidation schemes was found in this campaign.

382 Overall, a large part of missing OH sources was not explained by the isoprene chemistry. In the future, the impact of OVOCs  
383 species which was another potential OH source on missing OH sources need to be further evaluated.

384

### 385 **4.3 Sources and sinks of RO<sub>x</sub>**

386 The detailed analysis of radical sources and sinks was crucial to exploring radical chemistry. The experimental budget for HO<sub>2</sub>  
387 and RO<sub>2</sub> radicals could not be conducted because RO<sub>2</sub> was not measured during this campaign. Herein, we showed the  
388 simulated results by the base model. Figure 6 illustrates the diurnal profiles of RO<sub>x</sub> primary production rate ( $P(\text{RO}_x)$ ) and  
389 termination rate ( $L(\text{RO}_x)$ ), and the contributions of different channels during the daytime.



390

391 **Figure 6: The diurnal profiles of ROx primary production rate (a) and termination rate (b) simulated by the base model, and the**  
 392 **contributions of different channels to ROx primary production rate (c) and termination rate (d) during the daytime (08:00-18:00).**  
 393 **The grey areas denote nighttime.**

394 The ROx primary production and termination rates were basically in balance for the entire day, with maxima of  $4 \text{ ppb h}^{-1}$   
 395 around noontime. The ROx primary production rate was similar to those at Heshan ( $4 \text{ ppb h}^{-1}$ ) and Wangdu ( $5 \text{ ppb h}^{-1}$ ) sites,  
 396 but lower than those at Backgarden ( $11 \text{ ppb h}^{-1}$ ), Yufa ( $7 \text{ ppb h}^{-1}$ ), and Chengdu ( $7 \text{ ppb h}^{-1}$ ) sites (Lu et al., 2013; Lu et al.,  
 397 2012; Tan et al., 2017; Tan et al., 2019; Yang et al., 2021). During the daytime, the  $P(\text{ROx})$  mainly came from the OH and  $\text{HO}_2$   
 398 primary production. HONO and  $\text{O}_3$  photolysis dominated the OH primary production, and HCHO photolysis dominated the  
 399  $\text{HO}_2$  primary production. Thus,  $P(\text{ROx})$  was dominated by the photolysis reactions, in which the photolysis of HONO,  $\text{O}_3$ ,  
 400 HCHO, and carbonyls accounted for 29%, 16%, 16%, and 11% during the daytime, respectively. In the early morning, HONO  
 401 photolysis was the most important primary source of ROx, and the contribution of  $\text{O}_3$  photolysis became progressively larger  
 402 and was largest at noontime. A large discrepancy between the ratio of HONO photolysis rate to  $\text{O}_3$  photolysis rate in  
 403 summer/autumn and that in winter occurs generally. The vast majority of OH photolysis source is attributed to HONO  
 404 photolysis in winter because of the higher HONO concentration and lower  $\text{O}_3$  concentration. About half of  $L(\text{ROx})$  came from  
 405 OH termination, which occurred mainly in the morning, and thereafter, radical self-combination gradually became the major  
 406 sink of ROx in the afternoon. OH +  $\text{NO}_2$ , OH + NO, and OH + others contributed 35%, 5%, and 9% to  $L(\text{ROx})$ , respectively.  
 407  $\text{HO}_2 + \text{HO}_2$  and  $\text{HO}_2 + \text{RO}_2$  accounted for 8% and 16% in  $L(\text{ROx})$ .

#### 408 4.4 AOC evaluation

409 AOC controls the abundance of precursors and the production of secondary pollutants (Yang et al., 2020b; Elshorbany et al.,  
 410 2009), and thus it is necessary to quantify AOC for understanding photochemical pollution. The AOC has been evaluated in  
 411 previous studies, as shown in Table 1. Overall, the AOC values in summer are higher than those in autumn and winter, and the



412 values at lower latitudes are higher than those at higher latitudes for the same season. The vast majority of AOC in previous  
 413 studies are evaluated based on the non-observed radical concentrations.

414 **Table 1: Summary of OH concentrations and AOC values reported in previous field campaigns.**

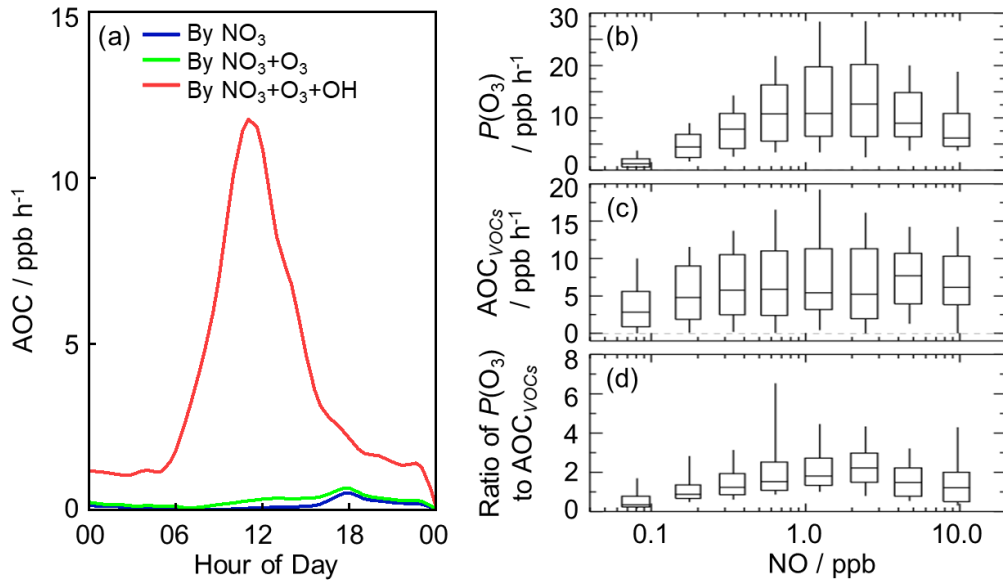
Location	Season, year	Site	Observed or non-observed radicals	of OH molecules $\text{cm}^{-3} \text{s}^{-1}$	AOC / $10^8$	References
Beijing, China	summer, 2018	urban	non-observed values		0.89 <sup>a</sup>	(Liu et al., 2021)
Beijing, China	summer, 2018	suburban	non-observed values		0.85 <sup>a</sup>	(Liu et al., 2021)
Beijing, China	winter, 2018	urban	non-observed values		0.21 <sup>a</sup>	(Liu et al., 2021)
Beijing, China	winter, 2018	suburban	non-observed values		0.16 <sup>a</sup>	(Liu et al., 2021)
Hongkong, China	summer, 2011	suburban	non-observed values		2.04 <sup>a,b</sup>	(Xue et al., 2016)
Santiago, Chile	summer, 2005	urban	non-observed values		3.4 <sup>a</sup>	(Elshorbany et al., 2009)
Hong Kong, China	late summer, 2012	coastal	non-observed values		1.4 <sup>c</sup>	(Li et al., 2018)
Hong Kong, China	autumn, 2012	coastal	non-observed values		0.62 <sup>c</sup>	(Li et al., 2018)
Hong Kong, China	winter, 2012	coastal	non-observed values		0.41 <sup>c</sup>	(Li et al., 2018)
Shanghai, China	summer, 2018	urban	non-observed values		1.0 <sup>c</sup>	(Zhu et al., 2020)
Berlin, Germany	summer, 1998	suburban	non-observed values		0.14 <sup>d</sup>	(Geyer et al., 2001)
Xianghe, China	autumn, 2019	suburban	non-observed values		0.49 <sup>c</sup>	(Yang et al., 2020b)
Beijing, China	summer, 2014	urban	non-observed values		1.7 <sup>a</sup>	(Feng et al., 2021)

415 Note that:

416 <sup>a</sup> Peak values in the diurnal profiles; <sup>b</sup> Values on 25 August 2021; <sup>c</sup> Maximum over a period of time; <sup>d</sup> Maximum on some day.

417 Herein, we explored the AOC in Shenzhen based on the observed radical concentrations for the first time. As illustrated in  
 418 Fig. 7 (a), the diurnal profile of AOC exhibits a unimodal pattern, which is the same as the diurnal profile of OH concentration  
 419 and  $j(\text{NO}_2)$ , with a peak around noontime. The diurnal peak of AOC was  $0.75 \times 10^8$  molecules  $\text{cm}^{-3} \text{s}^{-1}$  (11.8 ppb  $\text{h}^{-1}$ ).  
 420 Comparatively, AOC in this study can be comparable to those evaluated in Beijing (summer, 2018) and Hong Kong (autumn,  
 421 2012) (Li et al., 2018; Liu et al., 2021), but much lower than those evaluated in Hong Kong (summer, 2011) and Santiago  
 422 (summer, 2005) (Xue et al., 2016; Elshorbany et al., 2009).

423



424  
 425 **Figure 7: (a) The diurnal profiles of AOC in this campaign. (b) NO dependence of  $P(O_3)$  during the daytime. (c) NO dependence**  
 426 **of  $AOC_{VOCs}$  during the daytime, and  $AOC_{VOCs}$  denotes the atmospheric oxidation capacity only from the VOCs oxidation. (d) NO**  
 427 **dependence of the ratio of  $P(O_3)$  to  $AOC_{VOCs}$  during the daytime. The box-whisker plots in (b-d) give the 10%, 25%, median, 75%,**  
 428 **and 90%  $P(O_3)$ ,  $AOC_{VOCs}$  and the ratio of  $P(O_3)$  to  $AOC_{VOCs}$ , respectively.**

429 As expected, the dominant contributor to the AOC during this campaign was OH, followed by  $O_3$  and  $NO_3$ . Figure S4 shows  
 430 the fractional composition of the total AOC. The OH radical contributed about 95.7% of AOC during the daytime (08:00-  
 431 18:00).  $O_3$ , as the second important oxidant, accounted for only 2.9% of AOC during the daytime. The contribution of  $NO_3$  to  
 432 AOC during the daytime can be ignored, with a contribution of 1.4%. At night, the contributions of  $O_3$  and  $NO_3$  to AOC were  
 433 higher. OH,  $O_3$  and  $NO_3$  accounted for 75.7%, 6.4%, and 18% in the first half of night (18:00-24:00), and they accounted for  
 434 87.8%, 5%, and 7.3% in the second half of night (00:00-08:00).

435 As the indicator for secondary pollution, net  $O_3$  production rate,  $P(O_3)$ , can be calculated from the  $O_3$  formation rate ( $F(O_3)$ )  
 436 and the loss rate ( $L(O_3)$ ), as shown in Eq. (3-5) (Tan et al., 2017). The diurnal profiles of the speciation  $F(O_3)$  and  $L(O_3)$  were  
 437 shown in Fig. S5 in the Supplementary Information. The diurnal maxima of the modeled  $F(O_3)$  and  $L(O_3)$  were 18.9 ppb h<sup>-1</sup>  
 438 and 2.8 ppb h<sup>-1</sup>, with the maximum  $P(O_3)$  of 16.1 ppb h<sup>-1</sup> at 11:00. The modeled  $P(O_3)$  was comparable to that in Wangdu site  
 439 in summer and much higher than that in Beijing in winter (Tan et al., 2017; Tan et al., 2018).

$$440 F(O_3) = k_{HO_2+NO}[HO_2][NO] + \sum_i k_{RO_2i+NO}[RO_2]_i[NO] \quad (3)$$

$$441 L(O_3) = \theta j(O^1D)[O_3] + k_{O_3+OH}[O_3][OH] + k_{O_3+HO_2}[O_3][HO_2] + (\sum(k_{alkenes+O_3}^i[alkenes^i]))[O_3] \quad (4)$$

$$442 P(O_3) = F(O_3) - L(O_3) \quad (5)$$

443 where  $\theta$  is the fraction of  $O^1D$  from ozone photolysis that reacts with water vapor.

444 Herein, we presented the NO dependence of  $P(O_3)$ ,  $AOC_{VOCs}$ , and the ratio of  $P(O_3)$  to  $AOC_{VOCs}$  in Fig. 7 (b-d), in which  
 445  $AOC_{VOCs}$  denotes the atmospheric oxidation capacity only from the VOCs oxidation. An upward trend  $P(O_3)$  was presented  
 446 with the increase of NO concentration when NO concentration was below 1 ppb, while a downward trend was shown with the

447 increase of NO concentration when NO concentration was above 1 ppb. In terms of the NO dependence of  $AOC_{VOCs}$ , no  
448 significant variation was found, indicating VOCs oxidation was weakly impacted by NO concentrations in this campaign.  
449 Since  $AOC_{VOCs}$  can represent the VOCs oxidant rate, and thus the ratio of  $P(O_3)$  to  $AOC_{VOCs}$  can reflect the yield of ozone  
450 production from VOCs oxidation. Similar to  $P(O_3)$ , the ratio increased with the increase of NO concentration when NO  
451 concentration was below 1 ppb. When NO concentration was above 1 ppb, the ratio decreased with the increase of NO  
452 concentration because  $NO_2$  became the sink of OH radicals gradually. The maximum of the ratios existed when NO  
453 concentration was approximately 1 ppb, with a median of about 2, indicating the yield of ozone production from VOCs  
454 oxidation was about 2 in this study.

455

## 456 **5 Conclusions**

457 The STORM field campaign was carried out at Shenzhen site in autumn 2018, providing the continuous OH and  
458  $HO_2^*$  observations in PRD since the Heshan campaign in 2014. The maximum diurnal OH and  $HO_2^*$  concentrations, measured  
459 by laser-induced fluorescence (LIF), were  $4.5 \times 10^6 \text{ cm}^{-3}$  and  $4.5 \times 10^8 \text{ cm}^{-3}$ , respectively. The observed OH concentration was  
460 equal to that measured at Heshan site but was lower than those measured in summer campaigns in China (Backgarden, Yufa,  
461 Wangdu, and Chengdu sites).

462 The base model (RACM2-LIM1) could reproduce the observed OH concentration before 10:00, and thereafter, OH was  
463 underestimated by the model when NO concentration dropped to low levels. The results of the radical experimental budget  
464 indicated that OH underestimation was likely attributable to an unknown missing OH source at low NO conditions. We  
465 diagnosed the missing OH source by sensitivity runs, and unclassical OH recycling was identified again. A constant mixing  
466 ratio of the numerical species, X, equivalent to 0.1 ppb NO, was added to the base model to achieve the agreement between  
467 the modeled and observed OH concentrations. Additionally, we found isoprene and OVOCs might closely influence the  
468 missing OH sources by comparing the composition of VOCs reactivity under the different NO intervals. Isoprene isomerization  
469 mechanism (LIM1) can explain approximately 7% of the missing OH sources, and no significant contribution of MACR and  
470 MVK oxidation was found. As another potential OH source, OVOCs species should be further explored to explain the  
471 remaining missing OH sources. As for  $HO_2$  radicals, the overestimation of  $HO_2^*$  concentration was found, indicating that  $HO_2$   
472 heterogeneous uptake might make a significant role in  $HO_2$  sinks.

473 The quantification of production and destruction channels of ROx radicals is essential to explore the chemical processes of  
474 radicals. The ROx primary production and termination rates were balanced for the entire day, with maxima of  $4 \text{ ppb h}^{-1}$ , similar  
475 to those in the Heshan and Wangdu sites. Photolysis channels dominated the ROx primary production rate. HONO,  $O_3$ , HCHO,  
476 and carbonyls photolysis accounted for 29%, 16%, 16%, and 11% during the daytime, respectively. The most fraction of ROx

477 termination rate came from the reaction of OH + NO<sub>2</sub> in the morning. The radical self-combination gradually became the major  
478 sink of RO<sub>x</sub> in the afternoon with the decreasing of NO concentrations. The reaction of OH + NO<sub>2</sub> and radical self-combination  
479 accounted for 35% and 24% during the daytime, respectively.

480 In this campaign, AOC exhibited well-defined diurnal patterns, with a peak of 11.8 ppb h<sup>-1</sup>. As expected, OH radicals, which  
481 were the dominant oxidant, accounted for 95.7% of the total AOC during the daytime. O<sub>3</sub> and NO<sub>3</sub> contributed 2.9% and 1.4%  
482 to total AOC during the daytime, respectively. The ratio of  $P(O_3)$  to AOC<sub>VOCs</sub> trended to increase and then decrease as NO  
483 concentration increased, demonstrating the non-linear relationship between O<sub>3</sub> production and VOCs oxidation. The maximum  
484 of the ratios existed when NO concentration was approximately 1 ppb, with a median of about 2, indicating that the yield of  
485 ozone production from VOCs oxidation was about 2 in this campaign.

486

487 **Data availability.** The data used in this study are available from the corresponding author upon request (k.lu@pku.edu.cn).

488

489 **Author contributions.** YH Zhang and KD Lu conceived the study. XP Yang analyzed the data and wrote the manuscript with  
490 inputs from KD Lu. XP Yang, XF Ma, Y Gao contributed to the measurements of the HO<sub>x</sub> concentrations. All authors  
491 contributed to the discussed results and commented on the manuscript.

492

493 **Competing interests.** The authors declare that they have no conflict of interest.

494

495 **Acknowledgment.** The authors thank the science teams of the STORM-2018 campaign. This work was supported by the  
496 Beijing Municipal Natural Science Foundation for Distinguished Young Scholars (JQ19031), the National Research Program  
497 for Key Issue in Air Pollution Control (2019YFC0214800), and the National Natural Science Foundation of China (Grants  
498 No. 91544225, 21522701, 91844301).

## 499 **Appendix A. Supplementary data**

## 500 **References**

- 501 Brocco, D., Fratarcangeli, R., Lepore, L., Petricca, M., and Ventrone, I.: Determination of aromatic hydrocarbons in urban air  
502 of Rome, Atmospheric Environment, 31, 557-566, 10.1016/s1352-2310(96)00226-9, 1997.
- 503 Ehhalt, D. H.: Photooxidation of trace gases in the troposphere, Physical Chemistry Chemical Physics, 1, 5401-5408,  
504 10.1039/a905097c, 1999.
- 505 Elshorbany, Y. F., Kurtenbach, R., Wiesen, P., Lissi, E., Rubio, M., Villena, G., Gramsch, E., Rickard, A. R., Pilling, M. J., and  
506 Kleffmann, J.: Oxidation capacity of the city air of Santiago, Chile, Atmospheric Chemistry and Physics, 9, 2257-2273,  
507 10.5194/acp-9-2257-2009, 2009.
- 508 Fan, S., Wang, A., Fan, Q., Liu, J., and Wang, B.: ATMOSPHERIC BOUNDARY LAYER CONCEPT MODEL OF THE

509 PEARL RIVER DELTA AND ITS APPLICATION, *Journal of Tropical Meteorology*, 21, 286-292, 2005.

510 Feng, T., Zhao, S. Y., Hu, B., Bei, N. F., Zhang, X., Wu, J. R., Li, X., Liu, L., Wang, R. N., Tie, X. X., and Li, G. H.: Assessment  
511 of Atmospheric Oxidizing Capacity Over the Beijing-Tianjin-Hebei (BTH) Area, China, *Journal of Geophysical Research-  
512 Atmospheres*, 126, 18, 10.1029/2020jd033834, 2021.

513 Fuchs, H., Holland, F., and Hofzumahaus, A.: Measurement of tropospheric RO<sub>2</sub> and HO<sub>2</sub> radicals by a laser-induced  
514 fluorescence instrument, *Review of Scientific Instruments*, 79, 10.1063/1.2968712, 2008.

515 Fuchs, H., Bohn, B., Hofzumahaus, A., Holland, F., Lu, K. D., Nehr, S., Rohrer, F., and Wahner, A.: Detection of HO<sub>2</sub> by laser-  
516 induced fluorescence: calibration and interferences from RO<sub>2</sub> radicals, *Atmospheric Measurement Techniques*, 4, 1209-1225,  
517 10.5194/amt-4-1209-2011, 2011.

518 Fuchs, H., Tan, Z., Hofzumahaus, A., Broch, S., Dorn, H.-P., Holland, F., Kuenstler, C., Gomm, S., Rohrer, F., Schrade, S.,  
519 Tillmann, R., and Wahner, A.: Investigation of potential interferences in the detection of atmospheric RO<sub>x</sub> radicals by laser-  
520 induced fluorescence under dark conditions, *Atmospheric Measurement Techniques*, 9, 1431-1447, 10.5194/amt-9-1431-2016,  
521 2016.

522 Fuchs, H., Acir, I. H., Bohn, B., Brauers, T., Dorn, H. P., Häsel, R., Hofzumahaus, A., Holland, F., Kaminski, M., Li, X., Lu,  
523 K., Lutz, A., Nehr, S., Rohrer, F., Tillmann, R., Wegener, R., and Wahner, A.: OH regeneration from methacrolein oxidation  
524 investigated in the atmosphere simulation chamber SAPHIR, *Atmos. Chem. Phys.*, 14, 7895-7908, 10.5194/acp-14-7895-2014,  
525 2014.

526 Fuchs, H., Albrecht, S., Acir, I.-H., Bohn, B., Breitenlechner, M., Dorn, H.-P., Gkatzelis, G. I., Hofzumahaus, A., Holland, F.,  
527 Kaminski, M., Keutsch, F. N., Novelli, A., Reimer, D., Rohrer, F., Tillmann, R., Vereecken, L., Wegener, R., Zaytsev, A.,  
528 Kiendler-Scharr, A., and Wahner, A.: Investigation of the oxidation of methyl vinyl ketone (MVK) by OH radicals in the  
529 atmospheric simulation chamber SAPHIR, *Atmospheric Chemistry and Physics*, 18, 8001-8016, 10.5194/acp-18-8001-2018,  
530 2018.

531 Fuchs, H., Tan, Z., Lu, K., Bohn, B., Broch, S., Brown, S. S., Dong, H., Gomm, S., Haeseler, R., He, L., Hofzumahaus, A.,  
532 Holland, F., Li, X., Liu, Y., Lu, S., Min, K.-E., Rohrer, F., Shao, M., Wang, B., Wang, M., Wu, Y., Zeng, L., Zhang, Y., Wahner,  
533 A., and Zhang, Y.: OH reactivity at a rural site (Wangdu) in the North China Plain: contributions from OH reactants and  
534 experimental OH budget, *Atmospheric Chemistry and Physics*, 17, 645-661, 10.5194/acp-17-645-2017, 2017.

535 Gao, M., Li, H., Li, Y., Wei, J., Sun, Y., He, L., and Huang, X.: Source characteristics of water-soluble organic matters in  
536 PM<sub>(2.5)</sub> in the winter of Shenzhen, *China Environmental Science*, 38, 4017-4022, 2018.

537 Geyer, A., Alicke, B., Konrad, S., Schmitz, T., Stutz, J., and Platt, U.: Chemistry and oxidation capacity of the nitrate radical  
538 in the continental boundary layer near Berlin, *Journal of Geophysical Research-Atmospheres*, 106, 8013-8025,  
539 10.1029/2000jd900681, 2001.

540 Heard, D. E. and Pilling, M. J.: Measurement of OH and HO<sub>2</sub> in the troposphere, *Chemical Reviews*, 103, 5163-5198,  
541 10.1021/cr020522s, 2003.

542 Hofzumahaus, A., Aschmutat, U., Hessling, M., Holland, F., and Ehhalt, D. H.: The measurement of tropospheric OH radicals  
543 by laser-induced fluorescence spectroscopy during the POPCORN field campaign, *Geophysical Research Letters*, 23, 2541-  
544 2544, 10.1029/96gl02205, 1996.

545 Hofzumahaus, A., Rohrer, F., Lu, K., Bohn, B., Brauers, T., Chang, C.-C., Fuchs, H., Holland, F., Kita, K., Kondo, Y., Li, X.,  
546 Lou, S., Shao, M., Zeng, L., Wahner, A., and Zhang, Y.: Amplified Trace Gas Removal in the Troposphere, *Science*, 324, 1702-  
547 1704, 10.1126/science.1164566, 2009.

548 Holland, F., Hessling, M., and Hofzumahaus, A.: IN-SITU MEASUREMENT OF TROPOSPHERIC OH RADICALS BY  
549 LASER-INDUCED FLUORESCENCE - A DESCRIPTION OF THE KFA INSTRUMENT, *Journal of the Atmospheric  
550 Sciences*, 52, 3393-3401, 10.1175/1520-0469(1995)052<3393:ismoto>2.0.Co;2, 1995.

551 Huang, X.-F., Sun, T.-L., Zeng, L.-W., Yu, G.-H., and Luan, S.-J.: Black carbon aerosol characterization in a coastal city in  
552 South China using a single particle soot photometer, *Atmospheric Environment*, 51, 21-28,  
553 <https://doi.org/10.1016/j.atmosenv.2012.01.056>, 2012a.

554 Huang, X.-F., Chen, D.-L., Lan, Z.-J., Feng, N., He, L.-Y., Yu, G.-H., and Luan, S.-J.: Characterization of organic aerosol in  
555 fine particles in a mega-city of South China: Molecular composition, seasonal variation, and size distribution, *Atmospheric*

556 Research, 114-115, 28-37, <https://doi.org/10.1016/j.atmosres.2012.05.019>, 2012b.

557 Jones, C. E., Hopkins, J. R., and Lewis, A. C.: In situ measurements of isoprene and monoterpenes within a south-east Asian  
558 tropical rainforest, *Atmospheric Chemistry and Physics*, 11, 6971-6984, 10.5194/acp-11-6971-2011, 2011.

559 Lelieveld, J., Butler, T. M., Crowley, J. N., Dillon, T. J., Fischer, H., Ganzeveld, L., Harder, H., Lawrence, M. G., Martinez,  
560 M., Taraborrelli, D., and Williams, J.: Atmospheric oxidation capacity sustained by a tropical forest, *Nature*, 452, 737-740,  
561 10.1038/nature06870, 2008.

562 Levy, H.: NORMAL ATMOSPHERE - LARGE RADICAL AND FORMALDEHYDE CONCENTRATIONS PREDICTED,  
563 *Science*, 173, 141-&, 10.1126/science.173.3992.141, 1971.

564 Li, K., Jacob, D. J., Liao, H., Shen, L., Zhang, Q., and Bates, K. H.: Anthropogenic drivers of 2013-2017 trends in summer  
565 surface ozone in China, *Proceedings of the National Academy of Sciences of the United States of America*, 116, 422-427,  
566 10.1073/pnas.1812168116, 2019.

567 Li, Z., Xue, L., Yang, X., Zha, Q., Tham, Y. J., Yan, C., Louie, P. K. K., Luk, C. W. Y., Wang, T., and Wang, W.: Oxidizing  
568 capacity of the rural atmosphere in Hong Kong, Southern China, *Science of the Total Environment*, 612, 1114-1122,  
569 10.1016/j.scitotenv.2017.08.310, 2018.

570 Liu, S., Li, X., Shen, X., Zeng, L., Huang, X., Zhu, B., Lin, L., and Lou, S.: Measurement and partition analysis of atmospheric  
571 OH reactivity in autumn in Shenzhen, *Acta Scientiae Circumstantiae*, 39, 3600-3610, 2019.

572 Liu, Z., Wang, Y., Hu, B., Lu, K., Tang, G., Ji, D., Yang, X., Gao, W., Xie, Y., Liu, J., Yao, D., Yang, Y., and Zhang, Y.:  
573 Elucidating the quantitative characterization of atmospheric oxidation capacity in Beijing, China, *Science of the Total  
574 Environment*, 771, 10.1016/j.scitotenv.2021.145306, 2021.

575 Lou, S., Holland, F., Rohrer, F., Lu, K., Bohn, B., Brauers, T., Chang, C. C., Fuchs, H., Haeseler, R., Kita, K., Kondo, Y., Li,  
576 X., Shao, M., Zeng, L., Wahner, A., Zhang, Y., Wang, W., and Hofzumahaus, A.: Atmospheric OH reactivities in the Pearl  
577 River Delta - China in summer 2006: measurement and model results, *Atmospheric Chemistry and Physics*, 10, 11243-11260,  
578 10.5194/acp-10-11243-2010, 2010.

579 Lu, K., Guo, S., Tan, Z., Wang, H., Shang, D., Liu, Y., Li, X., Wu, Z., Hu, M., and Zhang, Y.: Exploring atmospheric free-  
580 radical chemistry in China: the self-cleansing capacity and the formation of secondary air pollution, *National Science Review*,  
581 6, 579-594, 10.1093/nsr/nwy073, 2019.

582 Lu, K. D., Hofzumahaus, A., Holland, F., Bohn, B., Brauers, T., Fuchs, H., Hu, M., Haeseler, R., Kita, K., Kondo, Y., Li, X.,  
583 Lou, S. R., Oebel, A., Shao, M., Zeng, L. M., Wahner, A., Zhu, T., Zhang, Y. H., and Rohrer, F.: Missing OH source in a  
584 suburban environment near Beijing: observed and modelled OH and HO<sub>2</sub> concentrations in summer 2006, *Atmospheric  
585 Chemistry and Physics*, 13, 1057-1080, 10.5194/acp-13-1057-2013, 2013.

586 Lu, K. D., Rohrer, F., Holland, F., Fuchs, H., Bohn, B., Brauers, T., Chang, C. C., Haeseler, R., Hu, M., Kita, K., Kondo, Y.,  
587 Li, X., Lou, S. R., Nehr, S., Shao, M., Zeng, L. M., Wahner, A., Zhang, Y. H., and Hofzumahaus, A.: Observation and modelling  
588 of OH and HO<sub>2</sub> concentrations in the Pearl River Delta 2006: a missing OH source in a VOC rich atmosphere, *Atmospheric  
589 Chemistry and Physics*, 12, 1541-1569, 10.5194/acp-12-1541-2012, 2012.

590 Ma, X., Tan, Z., Lu, K., Yang, X., Liu, Y., Li, S., Li, X., Chen, S., Novelli, A., Cho, C., Zeng, L., Wahner, A., and Zhang, Y.:  
591 Winter photochemistry in Beijing: Observation and model simulation of OH and HO<sub>2</sub> radicals at an urban site, *Science of the  
592 Total Environment*, 685, 85-95, 10.1016/j.scitotenv.2019.05.329, 2019a.

593 Ma, X. Y., Jia, H. L., Sha, T., An, J. L., and Tian, R.: Spatial and seasonal characteristics of particulate matter and gaseous  
594 pollution in China: Implications for control policy, *Environmental Pollution*, 248, 421-428, 10.1016/j.envpol.2019.02.038,  
595 2019b.

596 Mao, J., Ren, X., Zhang, L., Van Duin, D. M., Cohen, R. C., Park, J. H., Goldstein, A. H., Paulot, F., Beaver, M. R., Crounse,  
597 J. D., Wennberg, P. O., DiGangi, J. P., Henry, S. B., Keutsch, F. N., Park, C., Schade, G. W., Wolfe, G. M., Thornton, J. A., and  
598 Brune, W. H.: Insights into hydroxyl measurements and atmospheric oxidation in a California forest, *Atmospheric Chemistry  
599 and Physics*, 12, 8009-8020, 10.5194/acp-12-8009-2012, 2012.

600 Novelli, A., Hens, K., Ernest, C. T., Kubistin, D., Regelin, E., Elste, T., Plass-Duelmer, C., Martinez, M., Lelieveld, J., and  
601 Harder, H.: Characterisation of an inlet pre-injector laser-induced fluorescence instrument for the measurement of atmospheric  
602 hydroxyl radicals, *Atmospheric Measurement Techniques*, 7, 3413-3430, 10.5194/amt-7-3413-2014, 2014.

603 Peeters, J. and Muller, J.-F.: HOx radical regeneration in isoprene oxidation via peroxy radical isomerisations. II: experimental  
604 evidence and global impact, *Physical Chemistry Chemical Physics*, 12, 14227-14235, 10.1039/c0cp00811g, 2010.

605 Peeters, J., Nguyen, T. L., and Vereecken, L.: HOx radical regeneration in the oxidation of isoprene, *Physical Chemistry  
606 Chemical Physics*, 11, 5935-5939, 10.1039/b908511d, 2009.

607 Peeters, J., Muller, J.-F., Stavrou, T., and Vinh Son, N.: Hydroxyl Radical Recycling in Isoprene Oxidation Driven by  
608 Hydrogen Bonding and Hydrogen Tunneling: The Upgraded LIM1 Mechanism, *Journal of Physical Chemistry A*, 118, 8625-  
609 8643, 10.1021/jp5033146, 2014.

610 Ren, X., Olson, J. R., Crawford, J. H., Brune, W. H., Mao, J., Long, R. B., Chen, Z., Chen, G., Avery, M. A., Sachse, G. W.,  
611 Barrick, J. D., Diskin, G. S., Huey, L. G., Fried, A., Cohen, R. C., Heikes, B., Wennberg, P. O., Singh, H. B., Blake, D. R., and  
612 Shetter, R. E.: HOx chemistry during INTEX-A 2004: Observation, model calculation, and comparison with previous studies,  
613 *Journal of Geophysical Research-Atmospheres*, 113, 10.1029/2007jd009166, 2008.

614 Shu, L., Wang, T. J., Han, H., Xie, M., Chen, P. L., Li, M. M., and Wu, H.: Summertime ozone pollution in the Yangtze River  
615 Delta of eastern China during 2013-2017: Synoptic impacts and source apportionment, *Environmental Pollution*, 257,  
616 10.1016/j.envpol.2019.113631, 2020.

617 Stevens, P. S., Mather, J. H., Brune, W. H., Eisele, F., Tanner, D., Jefferson, A., Cantrell, C., Shetter, R., Sewall, S., Fried, A.,  
618 Henry, B., Williams, E., Baumann, K., Goldan, P., and Kuster, W.: HO<sub>2</sub>/OH and RO(2)/HO<sub>2</sub> ratios during the Tropospheric  
619 OH Photochemistry Experiment: Measurement and theory, *Journal of Geophysical Research-Atmospheres*, 102, 6379-6391,  
620 10.1029/96jd01704, 1997.

621 Stone, D., Whalley, L. K., and Heard, D. E.: Tropospheric OH and HO<sub>2</sub> radicals: field measurements and model comparisons,  
622 *Chemical Society Reviews*, 41, 6348-6404, 10.1039/c2cs35140d, 2012.

623 Stone, D., Evans, M. J., Walker, H., Ingham, T., Vaughan, S., Ouyang, B., Kennedy, O. J., McLeod, M. W., Jones, R. L.,  
624 Hopkins, J., Punjabi, S., Lidster, R., Hamilton, J. F., Lee, J. D., Lewis, A. C., Carpenter, L. J., Forster, G., Oram, D. E., Reeves,  
625 C. E., Bauguitte, S., Morgan, W., Coe, H., Aruffo, E., Dari-Salisburgo, C., Giammaria, F., Di Carlo, P., and Heard, D. E.:  
626 Radical chemistry at night: comparisons between observed and modelled HOx, NO<sub>3</sub> and N<sub>2</sub>O<sub>5</sub> during the RONOCO project,  
627 *Atmospheric Chemistry and Physics*, 14, 1299-1321, 10.5194/acp-14-1299-2014, 2014.

628 Tan, Z., Ma, X., Lu, K., Jiang, M., Zou, Q., Wang, H., Zeng, L., and Zhang, Y.: Direct evidence of local photochemical  
629 production driven ozone episode in Beijing: A case study, *Science of the Total Environment*, 800,  
630 10.1016/j.scitotenv.2021.148868, 2021.

631 Tan, Z., Lu, K., Hofzumahaus, A., Fuchs, H., Bohn, B., Holland, F., Liu, Y., Rohrer, F., Shao, M., Sun, K., Wu, Y., Zeng, L.,  
632 Zhang, Y., Zou, Q., Kiendler-Scharr, A., Wahner, A., and Zhang, Y.: Experimental budgets of OH, HO<sub>2</sub>, and RO<sub>2</sub> radicals and  
633 implications for ozone formation in the Pearl River Delta in China 2014, *Atmospheric Chemistry and Physics*, 19, 7129-7150,  
634 10.5194/acp-19-7129-2019, 2019.

635 Tan, Z., Fuchs, H., Lu, K., Hofzumahaus, A., Bohn, B., Broch, S., Dong, H., Gomm, S., Haeseler, R., He, L., Holland, F., Li,  
636 X., Liu, Y., Lu, S., Rohrer, F., Shao, M., Wang, B., Wang, M., Wu, Y., Zeng, L., Zhang, Y., Wahner, A., and Zhang, Y.: Radical  
637 chemistry at a rural site (Wangdu) in the North China Plain: observation and model calculations of OH, HO<sub>2</sub> and RO<sub>2</sub> radicals,  
638 *Atmospheric Chemistry and Physics*, 17, 663-690, 10.5194/acp-17-663-2017, 2017.

639 Tan, Z., Rohrer, F., Lu, K., Ma, X., Bohn, B., Broch, S., Dong, H., Fuchs, H., Gkatzelis, G. I., Hofzumahaus, A., Holland, F.,  
640 Li, X., Liu, Y., Liu, Y., Novelli, A., Shao, M., Wang, H., Wu, Y., Zeng, L., Hu, M., Kiendler-Scharr, A., Wahner, A., and Zhang,  
641 Y.: Wintertime photochemistry in Beijing: observations of ROx radical concentrations in the North China Plain during the  
642 BEST-ONE campaign, *Atmospheric Chemistry and Physics*, 18, 12391-12411, 10.5194/acp-18-12391-2018, 2018.

643 Wang, T., Xue, L. K., Brimblecombe, P., Lam, Y. F., Li, L., and Zhang, L.: Ozone pollution in China: A review of concentrations,  
644 meteorological influences, chemical precursors, and effects, *Science of the Total Environment*, 575, 1582-1596,  
645 10.1016/j.scitotenv.2016.10.081, 2017.

646 Wang, W., Parrish, D. D., Li, X., Shao, M., Liu, Y., Mo, Z., Lu, S., Hu, M., Fang, X., Wu, Y., Zeng, L., and Zhang, Y.: Exploring  
647 the drivers of the increased ozone production in Beijing in summertime during 2005-2016, *Atmospheric Chemistry and Physics*,  
648 20, 15617-15633, 10.5194/acp-20-15617-2020, 2020.

649 Whalley, L. K., Edwards, P. M., Furneaux, K. L., Goddard, A., Ingham, T., Evans, M. J., Stone, D., Hopkins, J. R., Jones, C.

650 E., Karunaharan, A., Lee, J. D., Lewis, A. C., Monks, P. S., Moller, S. J., and Heard, D. E.: Quantifying the magnitude of a  
651 missing hydroxyl radical source in a tropical rainforest, *Atmospheric Chemistry and Physics*, 11, 7223-7233, 10.5194/acp-11-  
652 7223-2011, 2011.

653 Whalley, L. K., Slater, E. J., Woodward-Massey, R., Ye, C., Lee, J. D., Squires, F., Hopkins, J. R., Dunmore, R. E., Shaw, M.,  
654 Hamilton, J. F., Lewis, A. C., Mehra, A., Worrall, S. D., Bacak, A., Bannan, T. J., Coe, H., Percival, C. J., Ouyang, B., Jones,  
655 R. L., Crilley, L. R., Kramer, L. J., Bloss, W. J., Vu, T., Kotthaus, S., Grimmond, S., Sun, Y., Xu, W., Yue, S., Ren, L., Acton,  
656 W. J. F., Hewitt, C. N., Wang, X., Fu, P., and Heard, D. E.: Evaluating the sensitivity of radical chemistry and ozone formation  
657 to ambient VOCs and NO<sub>x</sub> in Beijing, *Atmospheric Chemistry and Physics*, 21, 2125-2147, 10.5194/acp-21-2125-2021, 2021.  
658 Xue, L., Gu, R., Wang, T., Wang, X., Saunders, S., Blake, D., Louie, P. K. K., Luk, C. W. Y., Simpson, I., Xu, Z., Wang, Z.,  
659 Gao, Y., Lee, S., Mellouki, A., and Wang, W.: Oxidative capacity and radical chemistry in the polluted atmosphere of Hong  
660 Kong and Pearl River Delta region: analysis of a severe photochemical smog episode, *Atmospheric Chemistry and Physics*,  
661 16, 9891-9903, 10.5194/acp-16-9891-2016, 2016.

662 Yang, X., Wang, H., Tan, Z., Lu, K., and Zhang, Y.: Observations of OH Radical Reactivity in Field Studies, *Acta Chimica*  
663 *Sinica*, 77, 613-624, 10.6023/a19030094, 2019.

664 Yang, X., Lu, K., Ma, X., Liu, Y., Wang, H., Hu, R., Li, X., Lou, S., Chen, S., Dong, H., Wang, F., Wang, Y., Zhang, G., Li, S.,  
665 Yang, S., Yang, Y., Kuang, C., Tan, Z., Chen, X., Qiu, P., Zeng, L., Xie, P., and Zhang, Y.: Observations and modeling of OH  
666 and HO<sub>2</sub> radicals in Chengdu, China in summer 2019, *The Science of the total environment*, 772, 144829-144829,  
667 10.1016/j.scitotenv.2020.144829, 2021.

668 Yang, Y., Wang, Y., Yao, D., Zhao, S., Yang, S., Ji, D., Sun, J., Wang, Y., Liu, Z., Hu, B., Zhang, R., and Wang, Y.: Significant  
669 decreases in the volatile organic compound concentration, atmospheric oxidation capacity and photochemical reactivity during  
670 the National Day holiday over a suburban site in the North China Plain, *Environmental Pollution*, 263, 114657,  
671 <https://doi.org/10.1016/j.envpol.2020.114657>, 2020a.

672 Yang, Y., Wang, Y., Yao, D., Zhao, S., Yang, S., Ji, D., Sun, J., Wang, Y., Liu, Z., Hu, B., Zhang, R., and Wang, Y.: Significant  
673 decreases in the volatile organic compound concentration, atmospheric oxidation capacity and photochemical reactivity during  
674 the National Day holiday over a suburban site in the North China Plain, *Environmental Pollution*, 263,  
675 10.1016/j.envpol.2020.114657, 2020b.

676 Yang, Y., Shao, M., Kessel, S., Li, Y., Lu, K., Lu, S., Williams, J., Zhang, Y., Zeng, L., Noelscher, A. C., Wu, Y., Wang, X., and  
677 Zheng, J.: How the OH reactivity affects the ozone production efficiency: case studies in Beijing and Heshan, China,  
678 *Atmospheric Chemistry and Physics*, 17, 7127-7142, 10.5194/acp-17-7127-2017, 2017.

679 Yu, D., Tan, Z., Lu, K., Ma, X., Li, X., Chen, S., Zhu, B., Lin, L., Li, Y., Qiu, P., Yang, X., Liu, Y., Wang, H., He, L., Huang,  
680 X., and Zhang, Y.: An explicit study of local ozone budget and NO<sub>x</sub>-VOCs sensitivity in Shenzhen China, *Atmospheric*  
681 *Environment*, 224, 117304, <https://doi.org/10.1016/j.atmosenv.2020.117304>, 2020.

682 Zhang, Y. H., Hu, M., Zhong, L. J., Wiedensohler, A., Liu, S. C., Andreae, M. O., Wang, W., and Fan, S. J.: Regional Integrated  
683 Experiments on Air Quality over Pearl River Delta 2004 (PRIDE-PRD2004): Overview, *Atmospheric Environment*, 42, 6157-  
684 6173, 10.1016/j.atmosenv.2008.03.025, 2008.

685 Zhu, J., Wang, S., Wang, H., Jing, S., Lou, S., Saiz-Lopez, A., and Zhou, B.: Observationally constrained modeling of  
686 atmospheric oxidation capacity and photochemical reactivity in Shanghai, China, *Atmospheric Chemistry and Physics*, 20,  
687 1217-1232, 10.5194/acp-20-1217-2020, 2020.

688